photonics

Article

Comparative Study of Ultra-Narrow-Mode Generation in Random Fiber Lasers Based on Different Fiber Types

Ilya D. Vatnik *, Oleg A. Gorbunov and Dmitry V. Churkin

Physics Department, Novosibirsk State University, 630090 Novosibirsk, Russia
* Correspondence: i.vatnik@nsu.ru

Abstract: We studied the properties of ultra-narrow spectral modes, appearing in random distributed feedback Raman fiber lasers, for different fibers building up a laser cavity. Fibers with different nonlinear coefficients and dispersion were employed to obtain the generation. Ultra-narrow modes were observed in all fibers except those with the smallest dispersion. We measured the mode parameters, such as the average lifetime, as well as the maximum averaged output power that can support the ultra-narrow generation. The comparison revealed that the modes were more pronounced in high-dispersion fibers. Based on this comparative study, we conclude with the importance of the nonlinearity-dispersion interplay for regime stability.

Keywords: random feedback; random laser; Raman fiber laser

check for updates

Citation: Vatnik, I.D.; Gorbunov, O.A.; Churkin, D.V. Comparative Study of Ultra-Narrow-Mode Generation in Random Fiber Lasers Based on Different Fiber Types. *Photonics* **2023**, *10*, 1225. https://doi.org/10.3390/photonics10111225

Received: 3 October 2023
Revised: 26 October 2023
Accepted: 30 October 2023
Published: 1 November 2023

1. Introduction

Laser generation in fiber lasers with random distributed feedback, with a reflective element not localized but randomly distributed in space, is attractive due to its simplicity of implementation (if, for example, the inherent Rayleigh scattering in each fiber is used), outstanding lasing parameters, and variety of regimes achieved [1,2]. Rayleigh scattering by natural or artificial inhomogeneities plays the role of an array of random interferometers, which makes it possible to obtain narrow-band and single-frequency lasing [3,4]. A set of fiber Bragg gratings can also be used as a random reflector [5,6]. On the other hand, Raman lasers based on Rayleigh scattering become worthy rivals to standard Raman fiber lasers with point feedback, due to their high efficiency [7,8], and the possibility of obtaining high output powers [9,10] simultaneously with the ability to obtain lasing at various wavelengths [11,12]. The use of long sections of fibers as resonators, which provide a noticeable amount of integral backscattering, makes it possible, without the use of additional filter elements, to increase the brightness of multimode laser sources due to the effect of optical cleaning [13]. Due to low temporal coherence, laser radiation can be used to generate random numbers [14,15], temporal ghost imaging [16], and speckle-free imaging [17] and is considered a promising source of radiation for inertial thermonuclear fusion [12]. The typical values of the generation spectrum width of a random fiber Raman laser high above the threshold are a few nanometers, which at a wavelength of 1.5 μm, correspond to a characteristic correlation time equal to the inverse spectrum width of the order of 1–10 ps.

Recently, it was shown that a random fiber Raman laser can generate radiation with a significantly higher degree of coherence. The regime is observable near the generation threshold and leads to the generation of many narrow spectral modes arising simultaneously, each having a linewidth of less than 3 MHz [18]. The position of each mode in the spectrum is random, and modes exist for a limited time (about 1–10 ms). Notably, similar regimes imposed by Rayleigh backscattering causing random cavities are more easily observed in other types of random fiber lasers. For instance, the regime is found in a random laser with gain, owing to a semiconductor amplifier, in which modes also appeared for short times of the order of 1 ms, with the measured mode width being less than 10 kHz [19,20], as well as in random stimulated Brillouin scattering fiber lasers, which generate radiation with a spectral width down to several hertz [21].

The narrow-mode generation regime, appearing in random fiber Raman lasers, is possibly applicable to super-resolution spectroscopy [22]. In this technique aiming to reconstruct a fine spectral response of an object under study, the moderate resolution of a spectrum analyzer is significantly enhanced, with repetitive measurements using a narrow-band irradiation source. Importantly, the wavelength of the source must be changed either deterministically, or randomly, across the spectral range of interest, making the random Raman fiber a good candidate in these applications.

Since the regime is not easily achieved in all configurations of a random fiber laser with Raman amplification, the relevant question concerns the conditions needed to achieve one, as well as to increase the mode's output powers, lifetime, and occurrence frequency. In particular, the issue of processes leading to the destruction of the regime with the transition to broadband generation with a continuous spectrum is of great importance. In reference [19], a model was proposed according to which the lifetimes of individual modes are apparently determined by external factors, such as thermal or acoustic noise, leading to the restructuring of random resonators. However, their effects have marginal dependence on pump power and cannot lead to the cessation of the generation of narrow lines, while narrow-band lasing occurs only in a certain region near the threshold [18]. Considering that, high above the threshold, the shape of the spectrum is determined by the nonlinear process of four-wave mixing [23], it can be assumed that the generation of narrow modes is destroyed due to nonlinear interactions [24]. However, a detailed picture of the processes leading to the disappearance of the generation regime of narrow modes remains unclear.

In this work, we performed a comparative study of the narrow-mode generation in random lasers based on fibers with different parameters, such as the Kerr nonlinear coefficient and dispersion. This allowed us to highlight the importance of particular nonlinear processes that define the properties of the narrow modes.

2. Materials and Methods

We employed the random fiber laser scheme with forward pumping (see Figure 1) to study narrow-mode generation in different types of fibers. A fiber Bragg grating with a central wavelength of 1550.3 nm and a spectral width of 0.3 nm was placed at one side of a fiber spool to reduce the lasing threshold. A quasi-continuous wave Raman fiber laser, operating at a wavelength of 1455 nm, pumped the cavity through a wavelength-division multiplexer. The output radiation of the pump laser had a spectral linewidth of ~0.2 nm, with fully uncorrelated spectral components, which is typical for long fiber lasers. Thus, the time domain characteristics of the laser are typical for the uncorrelated light source, which is the stochastic temporal behavior with a typical correlation time of ~35 ps. At the forward output (co-directional with the pump wave), another wavelength-division multiplexer 1455/1550 nm was placed, to remove the undepleted pump from the system. The WDM was followed by the powerful isolator to eliminate backscattering of the signal from the edge of the output connectors and the measurement system, and to ensure the purely random nature of the feedback forming the resonator. The absence of parasitic backscattering at the laser output was ensured using optical time domain reflectometry measurements.

We examined the lasing characteristics of random fiber Raman lasers based on fibers with different parameters. In addition to the conventional SMF-28e+ fiber (32 km, high anomalous dispersion, D = 20 ps $\times$ nm^{-1} $\times$ km^{-1}), we tested Truewave RS fibers (10 km, low anomalous dispersion, D = 4 ps $\times$ nm^{-1} $\times$ km^{-1}), Truewave XL (4 km weak normal dispersion, $D = -3$ ps $\times$ nm^{-1} $\times$ km^{-1}), Corning MetroCore (22 km, average normal dispersion, $D = -7$ ps $\times$ nm^{-1} $\times$ km^{-1}), Truewave Reach fibers (10 km, D = 7 ps $\times$ nm^{-1} $\times$ km^{-1}), as well as dispersion compensating fiber (DCF) spools (3.5 km extra high normal, $D = -142$ ps $\times$ nm^{-1} $\times$ km^{-1}). Notably, although lengths of the fibers forming the resonator were different, the power values for the threshold pump were comparable in all cases. All the estimated parameters of the fibers are summarized in Table 1. The recapture factor connecting the Rayleigh losses and the Rayleigh backscattering values had approximately the same value of 0.002 for all fibers under consideration, except the DCF fiber, which had a larger numerical aperture and, thus, a larger recapture coefficient of 0.006.

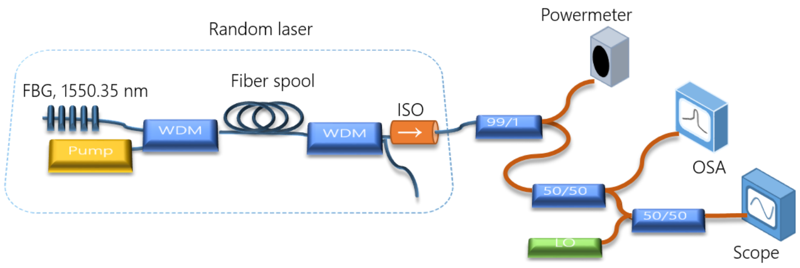

Figure 1. The experimental setup: FBG—fiber Bragg grating, WDM—wavelength division multiplexer, ISO—isolator, LO—local oscillator, OSA—optical spectrum analyzer.

Table 1. Parameters of the fiber spools utilized for a signal at 1550 nm.

Fiber Type	**Length, km**	**Dispersion, ps × nm^{-1} × km^{-1}**	**Kerr Nonlinearity, W^{-1} × km^{-1}**	**A_{eff}, μm^2**	**Losses, 1/km**
SMF-28e+	32	20	1.1	85	0.05
Truewave RS	10	4	1.7	~54	0.05
Truewave XL	4	−3	1.3	~70	0.05
Corning MetroCore	22	−7	1.5	~50	0.05
Truewave Reach	10	7	1.7	~55	0.05
Dispersion compensating fiber (DCF)	3.5	−142	4.4	~20	0.11

To establish the generation of localized modes, we used the grating-based single-pixel spectrometer Yokogawa AQ6370D. The spectrum in this device is measured by rotating the diffraction grating, which gives a low scanning speed (of the order of a nanometer per second). If a localized mode appears in the output generation during scanning, it is imprinted within the obtained spectrum with only a low probability; the generation of a localized mode (with a duration of a few milliseconds) with a certain wavelength must occur exactly at the moment when the spectrometer acquires power at this particular wavelength. To overcome this severe limitation, measurements using the standard spectrometer were carried out, in both the standard mode and in the “max hold” mode; to check the possibility of observing rare events of the generation of narrow modes, spectrum measurements were repeated 300 times, and for each wavelength, the maximum value of the spectral power density was retained over the entire spectra set. This approach made it possible to further confirm the presence of localized modes in the spectrum, as well as qualitatively compare the frequency of their occurrence for different fibers constituting the random lasers.

We also used optical heterodyning to study lasing spectra with high temporal resolution. For this purpose, the output radiation, after spectral filtering using an optical filter with a width of 4 GH at 1550.3 nm, was coupled with the radiation of a local oscillator—a tunable semiconductor laser PurePhotonics PCL550 with a generation wavelength of 1550.3 nm, an instantaneous linewidth of 10 kHz, and a long-term linewidth of the order of 2 MHz. The beat signal was measured using a balanced photodetector with a 20 GHz bandwidth and an oscilloscope with a 1 GHz bandwidth. The calibration of the measuring system using an auxiliary narrowband radiation helped in determining the amplitude-frequency characteristics of the measurement system and, thus, the reconstruction of the optical spectrum in a quantitative manner. To simplify the process of signal digitization, only a small part of the spectrum was derived, lying in the frequency band of ~60 MHz next to the carrier frequency of the local oscillator.

3. Results and Discussion

The measurement results demonstrated that localized modes are observed not only in the SMF-28e+ fiber, but also in fibers with lower dispersion values: Corning MetroCore ($D = -7$ ps $\times$ nm^{-1} $\times$ km^{-1}), Truewave Reach fiber ($D = 7$ ps $\times$ nm^{-1} $\times$ km^{-1}), as well as dispersion compensating fiber (DCF) spool ($D = -142$ ps $\times$ nm^{-1} $\times$ km^{-1}). At the same time, however, in Truewave fibers with a small dispersion value (normal and anomalous), the generation of localized modes was not observed (see Figure 2).

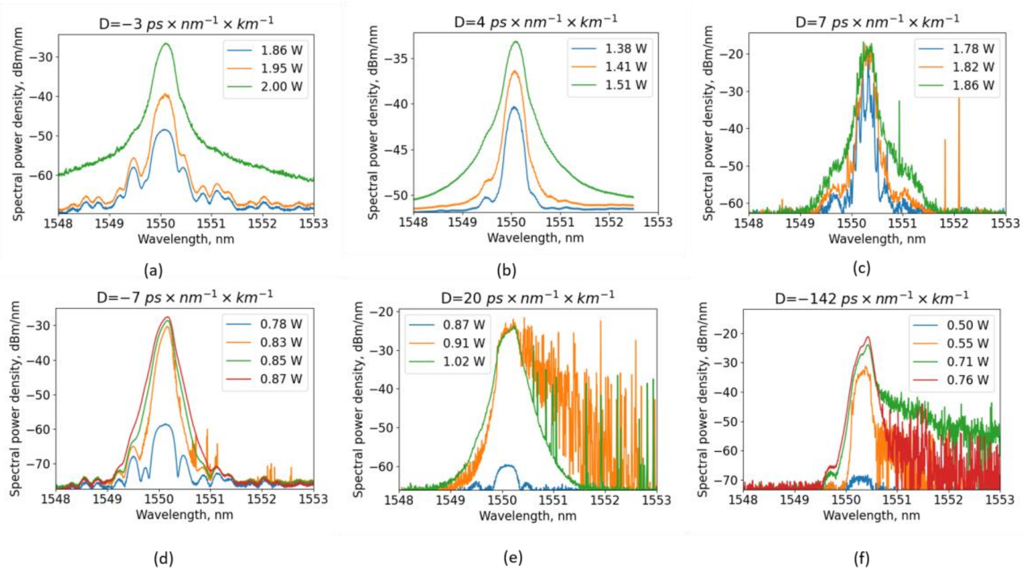

Figure 2. The generation spectra at the pump powers next to the threshold powers for fibers with different dispersion. Measurements are made in the "max hold" regime for: (**a**) Truewave XL (4 km, $D = -3$ ps $\times$ nm^{-1} $\times$ km^{-1}), (**b**) True Wave RS fibers (10 km, $D = 4$ ps $\times$ nm^{-1} $\times$ km^{-1}), (**c**) Truewave Reach fiber (10 km, $D = 7$ ps $\times$ nm^{-1} $\times$ km^{-1}), (**d**) Corning MetroCore (25 km, $D = -7$ ps $\times$ nm^{-1} $\times$ km^{-1}), (**e**) Corning SMF-28e+ (32 km, $D = 20$ ps $\times$ nm^{-1} $\times$ km^{-1}), and (**f**) dispersion compensating fiber (DCF) spool (3.5 km, $D = -142$ ps $\times$ nm^{-1} $\times$ km^{-1}).

The difference in behavior may arise from the action of cross-phase modulation (XPM) with the pump. Indeed, it is known that the main mechanism of spectral broadening in Raman fiber lasers is the Kerr nonlinear process of four-wave mixing [23]. We can assume that a narrow-modes regime is limited by effective energy transfer from intense modes to other spectral components; it is implicitly characterized by the value of the nonlinear phase, obtained due to the self-phase (SPM) and cross-phase modulation (XPM) processes. XPM can occur due to an interaction either with other modes in the spectrum, or with a pump wave. Since the intensity of the pump wave is much higher than that of the generation modes, the XPM is much more effective per unit length. However, due to the significant difference in group velocities between pump and generation waves, XPM with pumps can occur only at the distance of walk-off length L_W [25]. Considering the pump spectrum width Δ of about 0.2 nm, we acquire a characteristic coherence time $\tau \sim \Delta^{-1} = 35$ ps. Then, the walk-off length is $L_W = \tau v_{gp} \times (v_{gp} - v_{gs})^{-1} \times v_{gs} \approx \tau \times (D \times \Delta\lambda)^{-1}$ [24], where v_{gs} and v_{gp} represent group velocities at generation and pump wavelengths correspondingly and $\Delta\lambda = 95$ nm is the difference in Stokes shift. The value of XPM with pump wave can be estimated as an additional phase shift $\varphi_{NL} \approx \gamma \times P \times L_W \sim \gamma P \tau \times (D \times \Delta\lambda)^{-1}$. For Truewave RS and XL with small dispersion values it gives $\varphi_{NL} \sim 0.5$, for SMF-28e+ DCF phase shifts are $\varphi_{NL} \sim 0.036$, and $\varphi_{NL} \sim 0.004$, respectively ($\gamma \sim 1$ W^{-1} $\times$ km^{-1} and $P \sim 1$ W are similar for all fibers except DCF). In the first case, walk-off length is large enough for a nonlinear interaction to decompose the narrow modes indicated in the significant phase increment; conversely, for SMF-28e+ and DCF fibers, the XPM with pump has a marginal influence due to its fast walk-off, so the modes do present in the spectrum. The rest of the fibers are characterized by moderate values of nonlinear phase increments, so modes are observed, though not as often as in the SMF-28e+ fiber with high dispersion.

To test this hypothesis, we studied generation processes in SMF-28 fibers of different lengths (11, 20, and 32 km). We found that, in fibers that are 11 km long, localized modes are not observable; in fibers that are 20 km long, mode generation occurs with a low probability compared to fibers that are 32 km long. Since increasing the fiber length leads to a decrease in the lasing threshold (from 1.52 W to 0.8 W) and a decrease in the effects of phase cross-modulation with the pump wave, we concluded that the ability to observe localized modes was influenced by the magnitude of nonlinear interactions with the pump.

Increasing the dispersion makes it easier to observe the modes and increases the power of each mode. Thus, an analysis of the instantaneous spectrum was carried out using the optical heterodyne method, showing that, in fibers with low dispersion, narrow modes are observed with worse contrast (see Figure 3a). Each mode is present together with a wide spectral pedestal, which appears apparently due to the nonlinear broadening of the spectrum. In lasers using fibers with higher dispersion, such as SMF-28e+ or DCF, the modes are more expressed (see Figure 3b). At the same time, more power is concentrated in each mode. Therefore, the stimulated Brillouin scattering (SBS) process occurs more actively in these fibers, as the large fiber lengths, together with small linewidths of the generated random modes, make the threshold of Brillouin scattering easy to overcome. In its turn, the SBS ensures that the power of the narrow modes is transferred to the longer wavelengths, thus a number of Brillouin Stokes modes at the red wing of the generation spectrum appear (see Figure 2e). We have previously shown that SBS actually plays a significant role in this lasing regime [26].

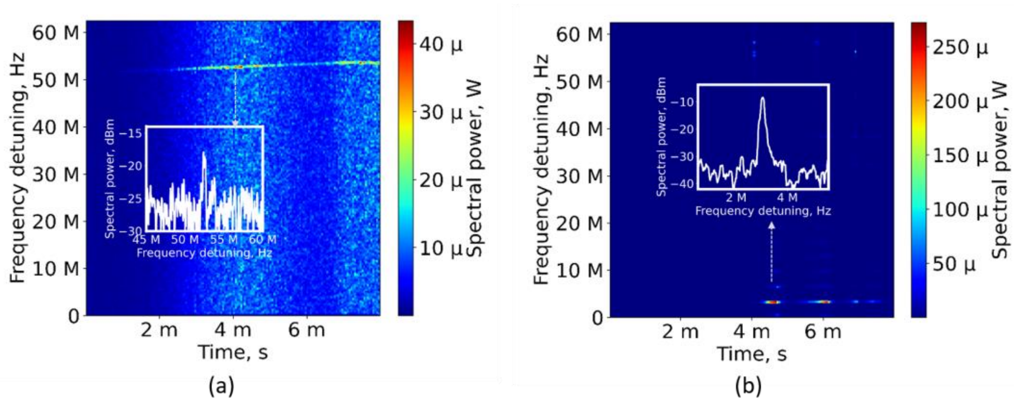

Figure 3. The experimentally obtained spectrograms revealing narrow mode dynamics in different fibers: (**a**) Truewave Reach (10 km, D = 7 ps $\times$ nm^{-1} $\times$ km^{-1}). Mode prominence is 6 dB (**b**) DCF (3.5 km, D = -142 ps $\times$ nm^{-1} $\times$ km^{-1}). Mode prominence >15 dB. Spectrograms measured at the pump powers of 1.79 W and 0.54 W correspondingly (next to generation threshold).

In fibers that support the generation of narrow spectral components, we measured the characteristic lifetimes. To calculate these, we employed the optical heterodyning method, repeatedly measuring the generation spectrum. Each measurement provided the time dependence of a specific narrow portion of the generation spectrum, similar to those shown in the spectrograms illustrated in Figure 3. In each spectrogram, a narrow mode with strong intensity was identified, and the time-dependent power within a small spectral range corresponding to that mode was derived. We defined the moments of mode initiation and cessation as the instances when the spectral power reached twice the level of background noise. Lifetime statistics were collected from 300 measurements for fibers with a high probability of obtaining the narrow modes (SMF-28e+, DCF). For fibers in which modes were observed less frequently (Truewave Reach, Metrocore), statistics were collected from several measurements.

We found that lifetimes depended only slightly on the type and length of the fiber. In all cases, the characteristic lifetime of the modes was of the order of several milliseconds (see two examples of probability distribution in Figure 4). Therefore, lifetimes can be determined not only using nonlinear effects, but also by using other factors, for example, using external noise, which leads to the restructuring of random microcavities [19,27,28]. It is noteworthy that profound differences in the dispersion between SMF-28e+ and DCF fibers were not manifested in the modes' lifetime at all.

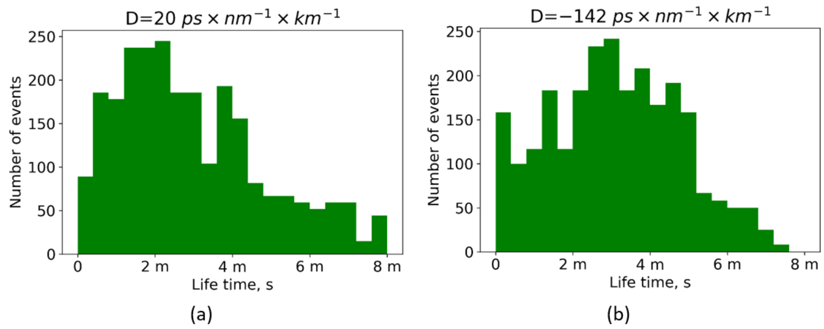

Figure 4. Statistics for the lifetimes of the narrow modes acquired for different fibers: (**a**) SMF-28e+ fiber, 32 km, D = 20 ps $\times$ nm^{-1} $\times$ km^{-1}, and (**b**) DCF, 3.5 km, $D = -142$ ps $\times$ nm^{-1} $\times$ km^{-1}.

We found that, in all lasers, the modes were observed in the same range of output lasing powers (see Figure 5). This is consistent with the assumption that the generation of narrow modes ceases to be observed at high lasing powers due to nonlinear effects. To further prove the assumption, we can estimate the nonlinear phase shift added to a mode amplitude owing to Kerr nonlinearity through SPM, indicating the degree of influence of nonlinear interactions. The general formula for phase increment in this case is $\varphi_{NL} = \int \gamma \times I(z) \times dz \approx \gamma_s \cdot I \cdot L_{\text{eff}}$, where $I(z)$ is the mode's intensity, z—fiber coordinate, and L_{eff}—effective fiber length. As the mode evolves for typically N~20 double cavity passes and its power can be estimated as 0.1–1 mW, we can conclude that L_{eff}~NL and φ_{NL}~0.1–1 indicate the major impact of nonlinear interactions. Note that a more accurate calculation of a maximum output power supporting nonlinear generation should take into account the influence of dispersion, which reduces the efficiency of the four-wave mixing process.

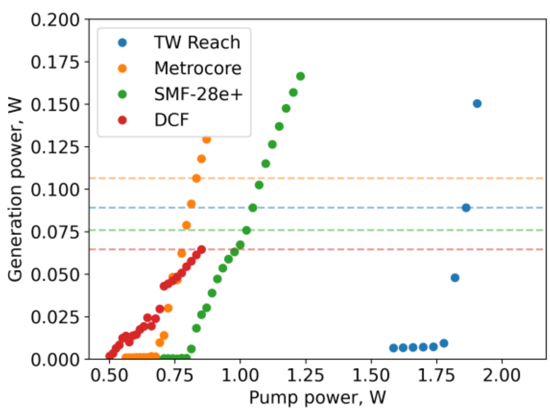

Figure 5. Output generation power as a function of pump power for four fiber spools, supporting the well-pronounced generation of the narrow modes. Dashed lines—the upper bounds of the range of output powers corresponding to the narrowband generation.

Finally, we estimated the impact of nonlinear effects by means of numerical simulations. For this, we performed a numerical simulation of laser generation in the fiber under study, just above the threshold. The employed numerical model [29] is based on the solution of a system of coupled nonlinear Schrödinger equations. The system is solved using a split-step method with iterative procedures, and output characteristics (spectra, etc.) are saved after every full cavity pass. The model takes into account all major physical processes: Raman gain, distributed optical feedback due to Rayleigh backscattering, chromatic dispersion, nonlinear effects, and linear attenuation, but does not consider the XPM between the pump and generation waves due to the extremely high computing time consumption.

The system of coupled nonlinear Schrödinger has the following representation:

$$\begin{cases} \frac{\partial A_p^+}{\partial z} - \frac{1}{\Delta v}\frac{\partial A_p^+}{\partial t} + \frac{i}{2}\beta_{2p}\frac{\partial^2 A_p^+}{\partial t^2} + \frac{\alpha_p}{2}A_p^+ = i\gamma_p\left|A_p^+\right|^2 A_p^+ - \frac{\hat{g}_p[\omega]}{2}\left(\left\langle\left|A_s^+\right|^2\right\rangle + \left\langle\left|A_s^-\right|^2\right\rangle\right)A_p^+ \\ \frac{\partial A_s^\pm}{\partial z} + \frac{i}{2}\beta_{2s}\frac{\partial^2 A_s^\pm}{\partial t^2} + \frac{\alpha_s}{2}A_s^\pm - \frac{\hat{\varepsilon}[\omega]}{2}A_s^\mp = i\gamma_s\left|A_s^\pm\right|^2 A_s^\pm - \frac{\hat{g}_s[\omega]}{2}\left(\left\langle\left|A_p^+\right|^2\right\rangle + \left\langle\left|A_p^-\right|^2\right\rangle\right)A_s^\pm \end{cases} \quad (1)$$

Here, indexes "*s*" and "*p*" are used for generating Stokes and pump waves, parameter A is a complex field envelope, t is the time in a frame of reference moving with the Stokes wave, z is a longitudinal coordinate being $z = 0$ for starting point of propagation, and $z = L$ at the other fiber end. Here, L is the fiber length, Δv is the difference between the pump and Stokes waves inverse group velocities, β_2, α, γ, g, and ε are dispersion, linear attenuation, and Kerr coefficients, respectively, and Raman gain coefficient and Rayleigh scattering coefficient, respectively (the last two are functions of frequency ω in the frequency domain, so they should be treated as operands in temporal representation). The sign $\pm$ denotes co- and counter-propagating waves. The parameters used in the simulations were taken from the technical datasheets of used fibers.

The value of the z-step is adaptive and, generally, there are several tens of thousands of coordinate steps on each iteration. The phase of the backscattered field is set to be δ-correlated in space; a chosen point in the fiber reflects light with a fixed phase, statistically independent of phases at different points. At the same time, the phases of the reflected light are chosen to be "frozen" in time and do not vary from one iteration to another.

The term with nonlinear coefficient γ describes the self-phase, cross-phase (inside its own spectrum), and four-wave mixing processes. In fact, these effects act together and cannot be separated inside the employed numerical model, but their efficiency can be estimated with the single parameter–nonlinear phase increment φ_{NL} described above. In fact, for narrow modes, spectral broadening occurs due to four-wave mixing, i.e., energy transfer from the pair spectral mode to two others [23]. We can identify the efficiency of this process by estimating a value φ_{NL}. The cross-phase modulation between the pump and generation waves can be described using the last term in the equations by omitting the averaging of the interacting waves.

As a test of the model, we compared the threshold pump powers predicted through the experiment and found good quantitative agreement.

For all fibers, the simulation predicts the presence of regimes of narrow generation, even for fibers where modes were not registered experimentally. This can be explained by the fact that the simulation does not consider an XPM with a pump wave and acts like an additional proof of XPM-induced mode demolition in fibers with low dispersion values.

In Figure 6, a spectrogram for the simulation of lasing in SMF-28e+ fibers is presented (pump power 0.98 W, total generation power 5.5 mW). The lifetimes of the modes were 2.6 ms, on average, which corresponded well to the experimental observations (Figure 4). The modes have a spectral width of a single frequency mesh step equal to 0.35 pm. Knowledge of the power distribution over the fiber during the simulation allows the calculation of nonlinear phase increments due to SPM effects, which appear to be of the order of unity. For example, for the narrow mode, presented in Figure 6b, the power I is 2.5 mW and the lifetime τ is about 2 ms, so the distance travelled in the fiber would be $L_{\text{eff}} \approx \tau c/n$~400 km with a nonlinear phase increment $\varphi_{NL} \approx \gamma_s \times I \times L_{\text{eff}}$~1 as $\gamma_s \approx 1\ \text{W}^{-1} \times \text{km}^{-1}$. This proves the importance of the Kerr nonlinearity, which starts to play an important role in mode dephasing at higher output powers.

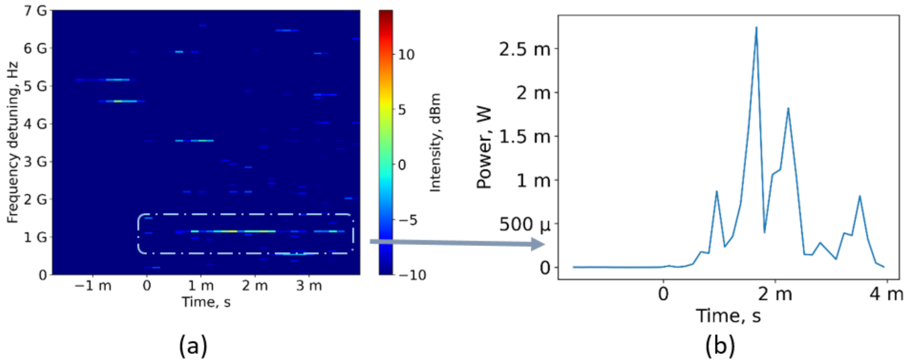

Figure 6. (**a**) The numerical simulation of the dynamics of the spectrum for the SMF-28e+ (32 km) fiber just above the generation threshold (pump power 0.98 W, total generation power 5.5 mW). (**b**) Simulated temporal dynamics of the mode output power, indicating the maximum mode output power of ~1 mW.

4. Conclusions

We have studied the generation of narrow spectral modes in a set of random fiber lasers, based on fibers with different dispersion and nonlinearity. Narrow modes have been detected for fibers with sufficiently high dispersion. In fibers with low dispersion, modes were difficult to observe, which may be attributed to the strong impact of Kerr phase cross-modulation with the pump wave. A comparison of the lifetimes of localized modes for fibers with different dispersion was carried out, and it was found that the lifetimes are the same in order of magnitude and do not depend on the dispersion value. Moreover, the generation of narrow modes is observed in comparable output power ranges, confirming the decisive role of nonlinear effects in the destruction of the mode. The numerical simulations demonstrated a qualitative agreement with the experiment for high-dispersion fibers and allowed us to estimate the nonlinear phase shifts for the modes, supporting the assumption of its essential role in the modes' regime disassembling.

Author Contributions: Conceptualization, I.D.V., O.A.G. and D.V.C.; methodology, I.D.V. and O.A.G.; writing—original draft preparation, I.D.V.; writing—review and editing, I.D.V., O.A.G. and D.V.C.; visualization, I.D.V.; supervision, I.D.V. and D.V.C.; project administration, D.V.C.; funding acquisition, D.V.C. All authors have read and agreed to the published version of the manuscript.

Funding: This research was funded by the Russian Science Foundation (19-12-00318-P, www.rscf.ru/project/22-12-35068/, accessed on 1 November 2023).

Institutional Review Board Statement: Not applicable.

Informed Consent Statement: Not applicable.

Data Availability Statement: The data underlying the results presented in this paper are not publicly available but may be obtained from the authors upon reasonable request.

Conflicts of Interest: The authors declare no conflict of interest.

References

1. Gomes, A.S.L.; Moura, A.L.; de Araújo, C.B.; Raposo, E.P. Recent Advances and Applications of Random Lasers and Random Fiber Lasers. *Prog. Quantum Electron.* **2021**, *78*, 100343. [CrossRef]
2. Chen, H.; Gao, S.; Zhang, M.; Zhang, J.; Qiao, L.; Wang, T.; Gao, F.; Hu, X.; Li, S.; Zhu, Y. Advances in Random Fiber Lasers and Their Sensing Application. *Sensors* **2020**, *20*, 6122. [CrossRef] [PubMed]
3. Skvortsov, M.I.; Abdullina, S.R.; Podivilov, E.V.; Vlasov, A.A.; Kharasov, D.R.; Fomiryakov, E.A.; Nikitin, S.P.; Treshchikov, V.N.; Babin, S.A. Extreme Narrowing of the Distributed Feedback Fiber Laser Linewidth Due to the Rayleigh Backscattering in a Single-Mode Fiber: Model and Experimental Test. *Photonics* **2022**, *9*, 590. [CrossRef]
4. Yin, G.; Saxena, B.; Bao, X. Tunable Er-Doped Fiber Ring Laser with Single Longitudinal Mode Operation Based on Rayleigh Backscattering in Single Mode Fiber. *Opt. Express* **2011**, *19*, 25981. [CrossRef] [PubMed]

5. Lizárraga, N.; Puente, N.P.; Chaikina, E.I.; Leskova, T.A.; Méndez, E.R. Single-Mode Er-Doped Fiber Random Laser with Distributed Bragg Grating Feedback. *Opt. Express* **2009**, *17*, 395. [CrossRef]
6. Rybaltovsky, A.; Popov, S.; Ryakhovskiy, D.; Abramov, A.; Umnikov, A.; Medvedkov, O.; Voloshin, V.; Kolosovskii, A.; Vorob'ev, I.; Chamorovskiy, Y.; et al. Random Laser Based on Ytterbium-Doped Fiber with a Bragg Grating Array as the Source of Continuous-Wave 976 Nm Wavelength Radiation. *Photonics* **2022**, *9*, 840. [CrossRef]
7. Liu, J.; Shen, D.; Huang, H.; Zhao, C.; Zhang, X.; Fan, D. High-Power and Highly Efficient Operation of Wavelength-Tunable Raman Fiber Lasers Based on Volume Bragg Gratings. *Opt. Express* **2014**, *22*, 6605–6612. [CrossRef]
8. Babin, S.A.; Zlobina, E.A.; Kablukov, S.I.; Podivilov, E.V. High-Order Random Raman Lasing in a PM Fiber with Ultimate Efficiency and Narrow Bandwidth. *Sci. Rep.* **2016**, *6*, 22625. [CrossRef]
9. Ma, R.; Li, J.Q.; Guo, J.Y.; Wu, H.; Zhang, H.H.; Hu, B.; Rao, Y.J.; Zhang, W.L. High-Power Low Spatial Coherence Random Fiber Laser. *Opt. Express* **2019**, *27*, 8738. [CrossRef]
10. Zhang, H.; Huang, L.; Song, J.; Wu, H.; Zhou, P.; Wang, X.; Wu, J.; Xu, J.; Wang, Z.; Xu, X.; et al. Quasi-Kilowatt Random Fiber Laser. *Opt. Lett.* **2019**, *44*, 2613. [CrossRef]
11. Gao, W.; Quan, X.; Ma, R.; Chen, Y.; Xu, S.; Wang, X.; Fan, D.; Liu, J. 10-Watt-Level 1.7 Mm Random Fiber Laser with Super-High Spectral Purity in a Cost-Effective and Robust Structure. *Photonics* **2022**, *9*, 900. [CrossRef]
12. Wang, P.; Lin, S.; Zhang, J.; Bao, X.; Ni, L.; Qi, Y.; Wang, Z. Efficient 1054 Nm Raman Random Fiber Laser. *Photonics* **2023**, *10*, 851. [CrossRef]
13. Chen, Y.; Fan, C.; Yao, T.; Xiao, H.; Xu, J.; Leng, J.; Zhou, P.; Kuznetsov, A.G.; Nemov, I.N.; Wolf, A.A.; et al. Comparison of Multimode GRIN-Fiber Raman Lasers with FBG and Random DFB Cavity. *J. Phys. Conf. Ser.* **2022**, *2249*, 012015. [CrossRef]
14. Monet, F.; Boisvert, J.-S.; Kashyap, R. A Simple High-Speed Random Number Generator with Minimal Post-Processing Using a Random Raman Fiber Laser. *Sci. Rep.* **2021**, *11*, 13182. [CrossRef] [PubMed]
15. Monet, F.; Kashyap, R. On Multiplexing in Physical Random Number Generation, and Conserved Total Entropy Content. *Sci. Rep.* **2023**, *13*, 7892. [CrossRef]
16. Wu, H.; Han, B.; Wang, Z.; Genty, G.; Feng, G.; Liang, H. Temporal Ghost Imaging with Random Fiber Lasers. *Opt. Express* **2020**, *28*, 9957. [CrossRef] [PubMed]
17. Ma, R.; Rao, Y.J.; Zhang, W.L.; Hu, B. Multimode Random Fiber Laser for Speckle-Free Imaging. *IEEE J. Sel. Top. Quantum Electron.* **2019**, *25*, 1–6. [CrossRef]
18. Kirik, A.E.; Vatnik, I.D.; Churkin, D.V. Direct Measurements of Localized Spectral Modes in Random Distributed Feedback Fiber Laser. *Results Phys.* **2021**, *28*, 104651. [CrossRef]
19. Tovar, P.; Temporão, G.; von der Weid, J.P. Longitudinal Mode Dynamics in SOA-Based Random Feedback Fiber Lasers. *Opt. Express* **2019**, *27*, 31001. [CrossRef]
20. Lima, B.C.; Tovar, P.; von der Weid, J.P. Generalized Extreme-Value Distribution of Maximum Intensities and Lévy-like Behavior in an SOA-Based Random Feedback Laser Emission. *J. Opt. Soc. Am. B* **2020**, *37*, 987. [CrossRef]
21. Pang, M.; Bao, X.; Chen, L. Observation of Narrow Linewidth Spikes in the Coherent Brillouin Random Fiber Laser. *Opt. Lett.* **2013**, *38*, 1866. [CrossRef] [PubMed]
22. Boschetti, A.; Taschin, A.; Bartolini, P.; Tiwari, A.K.; Pattelli, L.; Torre, R.; Wiersma, D.S. Spectral Super-Resolution Spectroscopy Using a Random Laser. *Nat. Photonics* **2020**, *14*, 177–182. [CrossRef]
23. Babin, S.A.; Churkin, D.V.; Ismagulov, A.E.; Kablukov, S.I.; Podivilov, E.V. Four-Wave-Mixing-Induced Turbulent Spectral Broadening in a Long Raman Fiber Laser. *JOSA B* **2007**, *24*, 1729. [CrossRef]
24. Fotiadi, A.A. Random Lasers: An Incoherent Fibre Laser. *Nat. Photonics* **2010**, *4*, 204–205. [CrossRef]
25. Agrawal, G.P. *Nonlinear Fiber Optics*; Academic Press: Cambridge, MA, USA, 2006; ISBN 978-0-12-369516-1.
26. Kirik, A.E.; Aprelov, N.A.; Vatnik, I.D.; Churkin, D.V. Observation of Cascade Brillouin Processes in Random Distributed Feedback Raman Fiber Lasers. In Proceedings of the Quantum and Nonlinear Optics IX; He, Q., Li, C.-F., Kim, D.-S., Eds.; SPIE: Cergy-Pontoise, France, 2023; p. 23. [CrossRef]
27. Tovar, P.; von der Weid, J.P. Dynamic Evolution of Narrow Spectral Modes in Stochastic Brillouin Random Fiber Lasers. *IEEE Photonics Technol. Lett.* **2021**, *33*, 1471–1474. [CrossRef]
28. Bliokh, Y.; Chaikina, E.I.; Vatnik, I.D.; Churkin, D.V. Temporal Variation of the Spectrum of a Continuously Pumped Random Fiber Laser: Phenomenological Model. *J. Opt. Soc. Am. B* **2019**, *36*, 408. [CrossRef]
29. Smirnov, S.V.; Churkin, D.V. Modeling of Spectral and Statistical Properties of a Random Distributed Feedback Fiber Laser. *Opt. Express* **2013**, *21*, 21236. [CrossRef]